Mechanical Systems and Signal Processing 86 (2017) 278–285

Contents lists available at ScienceDirect

Mechanical Systems and Signal Processing

journal homepage: www.elsevier.com/locate/ymssp

Circular geometric moiré for degradation prediction of mechanical components performing angular oscillations

P. Palevicius[a], A. Aleksa[a], R. Maskeliunas[b], M. Ragulskis[a,*]

[a] Research Group for Mathematical and Numerical Analysis of Dynamical Systems, Kaunas University of Technology, Studentu st. 50-146, LT-51368 Kaunas, Lithuania

[b] Department of Printing Machines, Vilnius Gediminas Technical University, J. Basanaviciaus st. 28-129, LT-03224 Vilnius, Lithuania

ARTICLE INFO

Keywords:
Geometric moiré
Angular oscillations
Degradation prediction

ABSTRACT

An experimental technique based on time-averaged circular geometric moiré for optical measurement of angular oscillations is presented in this paper. The pitch of the circular moiré is preselected in such a way that angular oscillations of different amplitudes yield time-averaged moiré fringes at different locations of the cover image. This optical effect enables to construct an optical scale for direct measurement of angular oscillations. The proposed technique is similar to visual cryptography, which is a cryptographic technique that allows encryption of visual information in such a way, that decryption can be done without use of any computational device. The efficiency and the applicability of the proposed technique for performance degradation prediction of rotating mechanical components is illustrated and validated by computational simulations and experimental tests.

1. Introduction

Time-averaged geometric moiré is a powerful optical experimental technique used for identification of in-plane deformations and strains [1]. Two basic goals exist in geometric moiré pattern analysis. The first problem is dedicated for the experimental interpretation of moiré patterns. In order to determine deformations, or strains at the centerlines of moiré fringes. Another objective is the inverse moiré pattern synthesis, when one has to generate two moiré gratings which yield the required moiré pattern when those gratings are superimposed [2,3]. Such superposition of transparent shares is an optical technique similar to visual cryptography.

Visual cryptography is a cryptographic technique that encrypts visual information (pictures, text, etc.). In case of visual cryptography, the decryption is a mechanical operation that can be performed without an aid of the computer. One of the first experimental implementation of visual cryptography has been proposed by Moni Naor and Adi Shamir [4]. In this scheme, an image was broken into n shares in such way, that only having all n shares would reveal the secret image, and $n-1$ shares would not leak any information about the secret image. The shares were printed on the transparent material and overlaying the shares revealed the secret image.

Various other techniques have been developed since the proposal of a method by Moni Naor and Adi Shamir. A halftone visual cryptography scheme was proposed that uses minimum auxiliary black pixels and provides uniform image quality [5]. This and similar methods decreases suspicion of secret image encryption since meaningful information is visible in the cover image. It allows

* Corresponding author.
E-mail addresses: paulius.palevicius@ktu.lt (P. Palevicius), algiment.alesa@ktu.lt (A. Aleksa), rimas.maskeliunas@vgtu.lt (R. Maskeliunas), minvydas.ragulskis@ktu.lt (M. Ragulskis).

http://dx.doi.org/10.1016/j.ymssp.2016.10.011
Received 9 May 2016; Received in revised form 12 September 2016; Accepted 9 October 2016
Available online 20 October 2016
0888-3270/

to hide the fact that information has been encoded in the first place. Similar techniques and approaches are also presented in [6–8].

Most visual cryptography techniques concentrate on binary images. Nevertheless, methods or schemes for processing grayscale and color images are being developed. A technique developed by [9] proposes three methods for visual cryptography of grayscale and color images based on binary visual cryptography, the halftone technology, and the color decomposition method. In many color visual cryptography techniques, larger pixel expansion is needed in order to produce more colors, but it has a negative impact on size. Thus a technique of additive color mixing in a probabilistic way and a new color visual cryptography scheme with the fixed pixel expansion was proposed in [10]. Though this method reduces contrast quality of decoded secret image. Another method that uses color transfer scheme and incorporates it into the (k, n) visual cryptography model is proposed in [11]. During encoding state, a color image is encrypted into n binary share images. When k or more than k shares are collected, a high quality colorful variation of the secret image is reconstructed.

Time-averaged geometric moiré is a dynamic alternative to static double exposure geometric moiré. A single moiré grating is used in time-averaged geometric moiré. An opaque image of the grating is printed on the surface of a oscillating body and time-averaging techniques are used to acquire time-averaged moiré fringes [12]. Exploitation of time-averaged geometric moiré is not limited to optical analysis of oscillating structures. It can be also used for the synthesis of a predefined pattern of time-averaged fringes. Such type of image hiding technique (when the secret image leaks in the form of a time-averaged moiré fringe in an oscillating non-deformable cover image) was first presented in [13]. The secret image is embedded into a single cover image by using a stochastic moiré grating. A visual decoding of the secret image can be performed by a human visual system if the amplitude of the harmonic oscillations corresponds to a preselected value. This visual cryptography technique requires only one image; the encoded image looks completely random in the state of the equilibrium. The secret image is visualized only at strictly defined parameters of oscillation. The fact that special algorithms are required to encode the secret in the cover image, and the human visual system can interpret the secret from a time-averaged image makes this image hiding technique similar to visual cryptography. The difference from visual cryptography is that only a single cover image is used and that it must be oscillated in order to leak the visual secret.

The main objective of this paper is to present an experimental technique for optical measurement of angular oscillations. Instead of hiding any secrets in the cover image, we construct a circular moiré grating with a variable pitch. Different amplitudes of angular oscillations yield time-averaged moiré fringes at different locations of the cover image in the time-averaged mode. This optical phenomenon is exploited for the construction of an optical scale for the measurement of the amplitude of angular oscillations and could be exploited for performance degradation prediction of rotating mechanical components. It is worth mentioning that there exist different experimental and analytical techniques for performance degradation prediction of rotating mechanical components. A multisensor system for in situ shape monitoring and damage identification of high-speed composite rotors is developed in [14]. A new approach to health monitoring and assessment of rolling bearing is proposed in [15]. A proportional hazard model employing support vector machines is used for machine performance degradation assesment [16]. Real-time assessment of remaining lifetime of bearings is performed using the individual state deviation based on the manifold distance [17]. Health assessment of rotary machinery based on integrated feature selection and Gaussian mixed model is proposed in [18]. As mentioned previously, this paper raises a similar objective to develop an experimental technique for performance degradation prediction of rotating mechanical components. However, the novelty of our approach is that the proposed experimental technique is completely optical and does not require mounting any additional sensors or instruments.

This paper is organized as follows. The formation of time-averaged moiré fringes and optical background is discussed in Section 2. An algorithm of image hiding scheme based on circular moiré grating is provided in Section 3. Experimental setup and results are given in Section 4. Concluding remarks are given in the final Section.

2. Optical background

Moiré grating on the surface of a one-dimensional structure in the state of equilibrium can be interpreted as a periodic variation of grayscale colors [1]:

$$M(y) = \frac{1}{2} + \frac{1}{2}\cos\left(\frac{2\pi}{\lambda}y\right) \tag{1}$$

where y is the longitudinal coordinate; $M(y)$ is grayscale level of the surface at point y; λ is the pitch of the grating. Values 0 and 1 of function $M(y)$ correspond to black and white colors respectively; intermediate values correspond to an appropriate grayscale color.

Let us assume that deflections from the sate of equilibrium oscillate in time and are defined as:

$$u(x, t) = a(x)\sin(\omega t + \phi) \tag{2}$$

where a is the amplitude of harmonic oscillations; ω is the circular frequency; ϕ is the phase. Then, the time-averaged image (when the exposure time T tends to infinity) reads [1]:

$$M_T(x, y) = \frac{1}{2} + \frac{1}{2}\cos\left(\frac{2\pi}{\lambda}y\right)J_0\left(\frac{2\pi}{\lambda}a(x)\right) \tag{3}$$

where J_0 is the zero order Bessel function of the first kind:

$$J_0(x) = \lim_{T\to\infty}\frac{1}{T}\int_0^T \exp(i\cdot x\sin t)dt \tag{4}$$

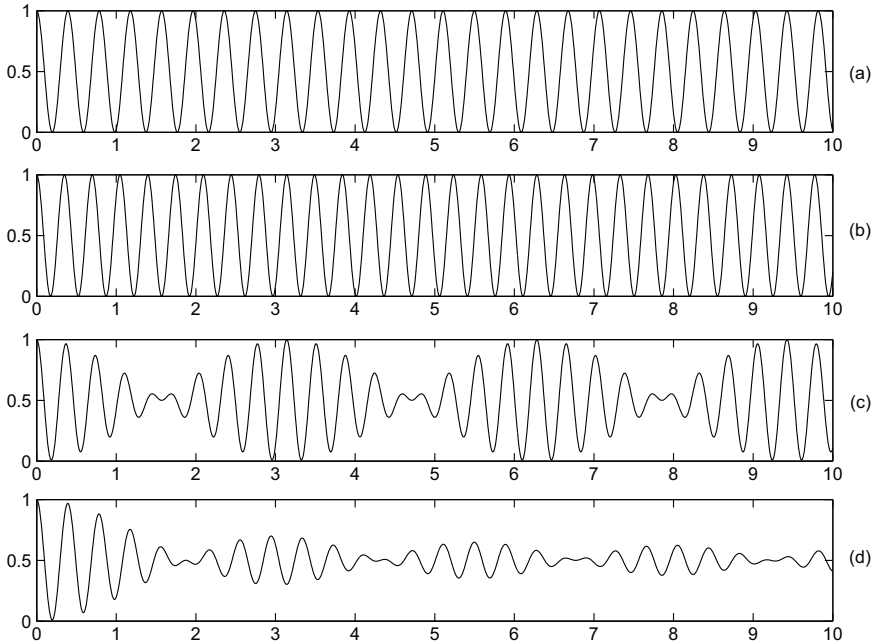

Fig. 1. The computational example of time-averaged moiré fringes: moiré grating in the state of equilibrium is shown in part (a), deformed grating is shown in part (b), double exposure of parts (a) and (b) is shown in part (c), and time-averaged image is shown in part (d).

The envelope function modulating the time-averaged blur induced by harmonic oscillations reads:

$$E(a(x))) = \frac{1}{2} \pm \frac{1}{2} J_0\left(\frac{2\pi}{\lambda} a(x)\right) \tag{5}$$

where J_0 is the zero order Bessel function of the first kind. Thus, time-averaged moiré fringes will form when:

$$J_0\left(\frac{2\pi}{\lambda} a(x)\right) = 0 \tag{6}$$

The relationship between the order of time-averaged fringe, the amplitude of harmonic oscillations and the pitch of moiré grating takes the following form:

$$\frac{2\pi}{\lambda} a_i(x) = r_i \tag{7}$$

where r_i denotes the i-th root of J_0; $a_i(x)$ is the amplitude of oscillation at the center of the i-th time-averaged fringe.

A stationary moiré grating with $\lambda = \pi/8$ is shown in Fig. 1 (a); a stationary grating at $\lambda = \pi/9$ is illustrated in Fig. 1(b). Double exposure of (a) and (b) gratings is shown in Fig. 1(c). The effect of beatings is visible in this image. Finally, the time-averaged image is shown in Fig. 1(d). Note, that harmonic oscillations of the deformable one-dimensional deformable moiré grating are considered in Fig. 1(d).

3. Image hiding scheme based on circular moiré grating

The objective of this paper is to construct a circular moiré grating which could be applicable measuring amplitude of angular oscillations, thus angular harmonic oscillations are now considered instead of longitudinal harmonic oscillations used in [13]. The cover image now is comprised of concentric circle around a fixed central point (x_0, y_0) where it corresponds to circular moiré grating. Concentric circle is designed as a set of grayscale pixels according to Eq. (1), where the longitudinal coordinate y is replaced by the angular coordinate φ; and unidirectional oscillations along the y-axis are replaced by angular oscillations around the central point (x_0, y_0). The assumption that the amplitude of harmonic angular oscillations a is constant in the area of the whole image yields:

$$M_T(x, y) = \lim_{n\to\infty} \frac{1}{n} \cdot \quad \cdot \sum_{k=0}^{n-1} \frac{1}{2}\left(1 + \cos\left(\frac{2\pi}{\lambda}\left(\varphi_0 + a \sin\left(\frac{2\pi k}{n}\right)\right)\right)\right) \tag{8}$$

where n is the number of discrete time nodes in a period of harmonic angular oscillations, and φ_0 is the angular coordinate of the current point (x, y) in respect to the central point of angular oscillations [19]:

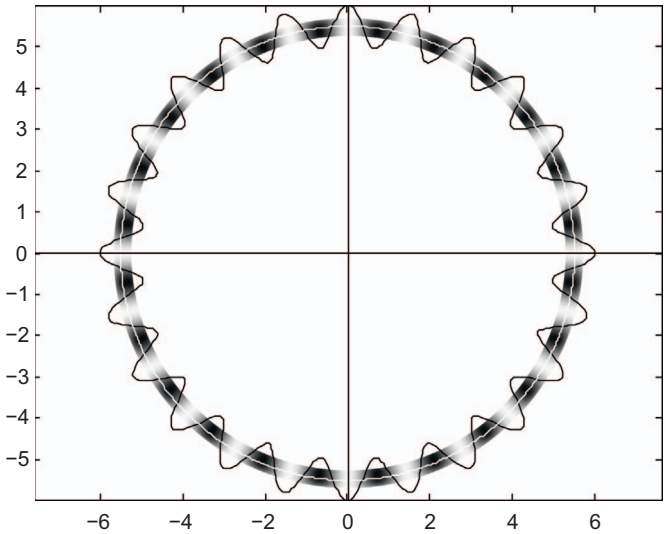

Fig. 2. Circular moiré grating with pitch $\lambda = \pi/12$ in the state of equilibrium.

$$\varphi_0 = \arctan\left(\frac{y_0 - y}{x - x_0}\right) \tag{9}$$

The formation of a static concentric moiré circle is illustrated in Fig. 2. The variation of the grayscale color in the angular direction is shown in thin solid line; the according optical interpretation of this variation is schematically illustrated as ring corresponding to this concentric moiré grating. Note that the angular pitch of the concentric moiré grating is selected in such a way, that an integer number of pitches would fit into whole circle.

It is clear that angular oscillations of the concentric moiré grating in Fig. 2 will produce time-averaged moiré fringes similar to ones illustrated in Fig. 1(d). Time-averaged optical effects (as the exposure time tends to infinity) are illustrated in Fig. 3. The amplitude of angular harmonic oscillations a increases along the horizontal axis: a=0 at the left part of the image (marked as (1) in Fig. 3); a=0.23 at marker (2); a=0.6 at marker (3). The increasing amplitude of angular oscillations results into motion induced blur in time-averaged image; yet the process is not monotonic at increasing amplitudes of oscillations. The concentric moiré circle is static at a=0 and is visualized in Fig. 3(b). The amplitude of angular oscillations at marker (2) is preselected in such a way, that it results into the second root of the zero order Bessel function of the first kind ($a = \frac{\lambda}{2\pi} r_2$). The time-averaged moiré fringe at marker (2) is illustrated in Fig. 3(c). Finally, the time-averaged image of the oscillating circular moiré grating at marker (3) is illustrated in Fig. 3(d).

Let us consider a circular geometric moiré grating with constant angular pitch Fig. 4 (a). It is clear that an appropriate selection of the amplitude of harmonic angular oscillations around the center-point of the circular moiré image would produce a time-averaged moiré fringe. However, this amplitude of harmonic oscillations must correspond to the root of the zero order Bessel function of the first kind Eq. (7). The resulting time-averaged moiré fringe is not fully developed or even not visible at all if the amplitude of harmonic oscillations does not correspond to the appropriate root of J_0 (Fig. 4(b)). Note, that time-averaged moiré fringe does form in the whole observation area and the grayscale color becomes equal to 0.5 in Fig. 4(c).

Such optical effect generated in the time-averaged mode offers a convenient approach for measuring amplitudes of angular oscillations. Let us consider a circular geometric moiré image where the angular pitch of the grating depends on the angular coordinate φ Fig. 5 (c). Then different amplitudes of angular oscillations will result into different locations of time-averaged moiré fringe. Fig. 5(a) demonstrates time-averaged image of the circular grating at a=0.024; Fig. 5(b) illustrates the highlighted time-averaged fringe where the time-averaged image is processed by grayscale color enhancement algorithm. Note, that the angle of the centerline of the time-averaged moiré fringe can be used as an optical detector of the oscillation amplitude. The same computational experiment is repeated at a=0.028 (Fig. 5(d) and (e)). The circular scale of amplitudes of angular oscillations corresponding to the circular grating is given in Fig. 5(c).

The relationship between the angular coordinate φ and the amplitude of angular oscillations a must be predetermined at the stage of the design of the angular scale. The angular pitch of the circular grating must be preselected in such a way, that the centerline of a time-averaged fringe would form a required angle with x-axis of the grating. In other words the angular scale is an integral part of the circular grating. This fact does not limit the applicability of such technique for measurement of angular oscillations – one does not need to specially orient the circular moiré grating in respect of any coordinate system. Even if the stationary image of the grating in 5(c) would be rotated by some angle, the centerline of produced fringe would still point to the correct reading of a.

Note, that the formation of time-averaged moiré fringes does not depend on the frequency of harmonic oscillations. The resulting time-averaged image does not depend on the angular frequency ω (Eq. (3)). In other words the proposed technique cannot detect

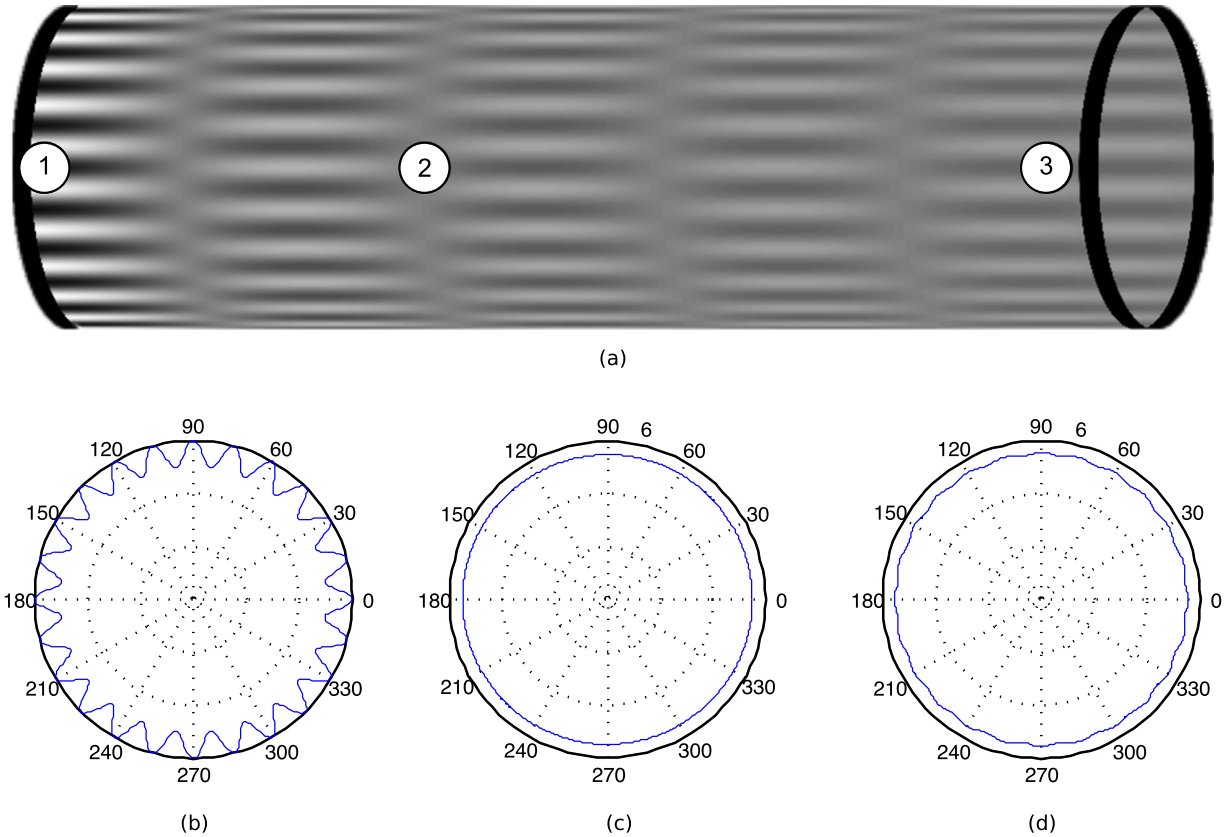

Fig. 3. The computational example of time-averaged circular moiré fringes performing angular oscillations with pitch $\lambda = \pi/12$: time-averaged fringes of angular oscillations with $a = 0\ldots0.6$ are shown in (a), time-averaged fringes corresponding to cross-sections Sections (1)–(3) in (a) are respectively shown in (b), (c) and (d).

any disturbances of the oscillation frequency if only the amplitude of oscillations is kept strictly constant.

A much more demanding situation would occur when the amplitude of angular oscillation is disturbed. Applicability of time-averaged moiré techniques for oscillations with chaotically varying amplitudes is investigated in details in [20]. Thus, the proposed technique can be used for optical identification of chaotic angular oscillations. So far, the proposed optical technique could only detect variations of the amplitude of harmonic angular oscillations. However, one can detect the presence of chaotic angular oscillations if the time-averaged image of the angular scale becomes blurred and it becomes difficult to determine the centerline of time-averaged moiré fringe.

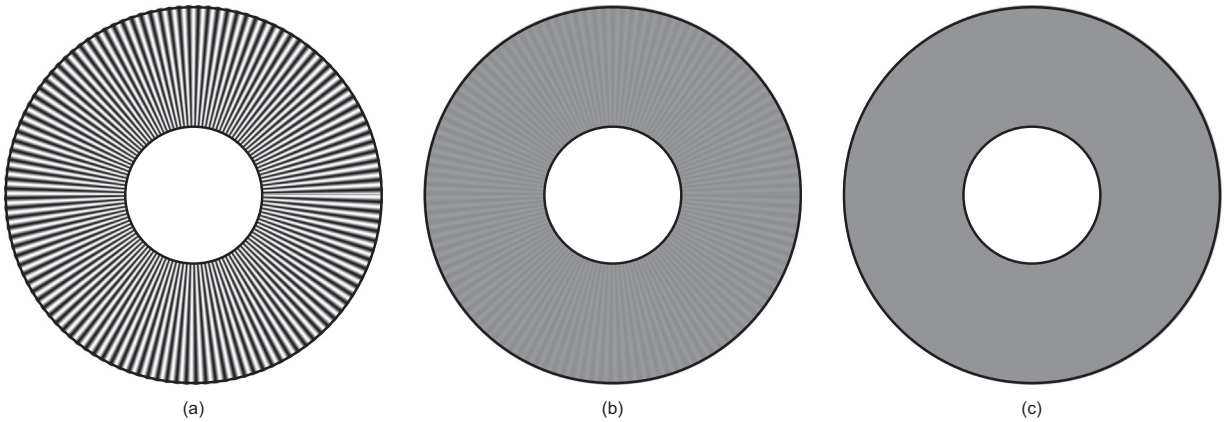

Fig. 4. A The computational example of time-averaged circular moiré fringes: circular moiré grating in the state of equilibrium is shown in part (a), undeveloped time-averaged fringes of angular oscillations with a=0.0191 are shown in part (b), and time-averaged fringes of angular oscillations with a=0.02 are shown in part (c),.

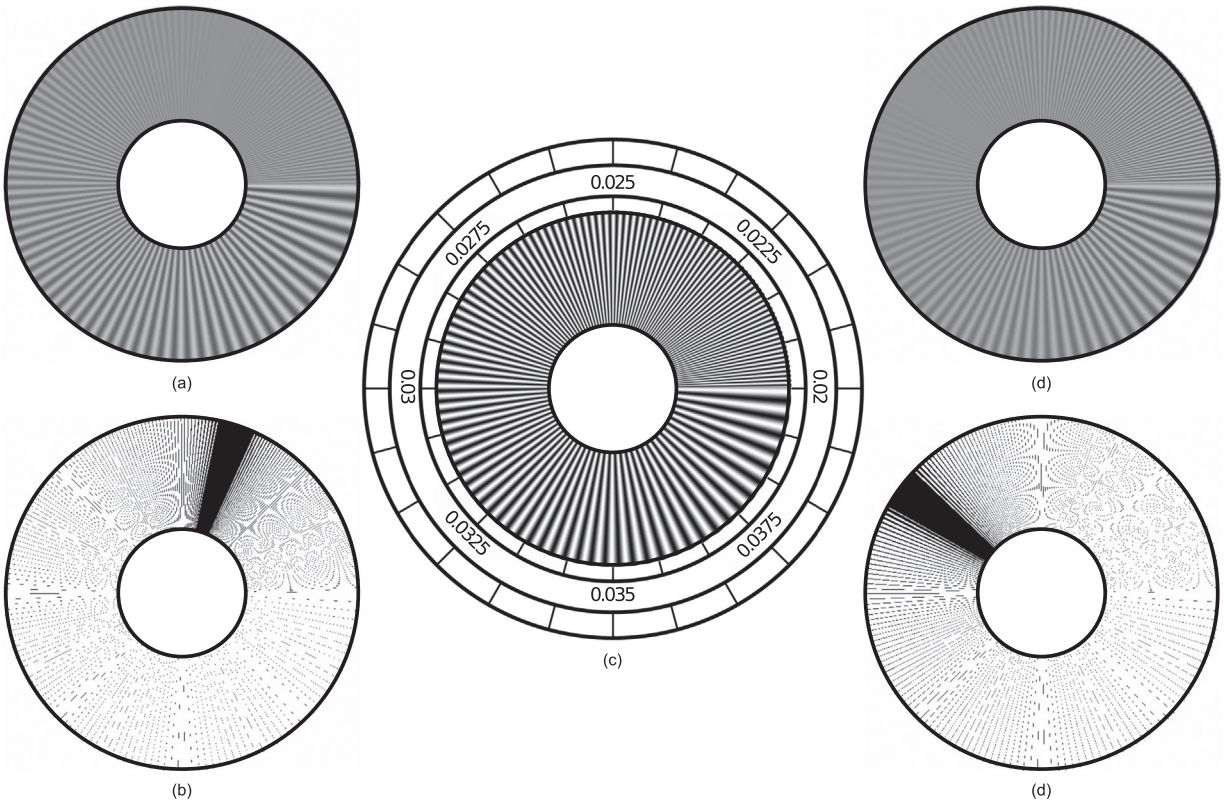

Fig. 5. The computational example of time-averaged circular moiré fringes: circular moiré grating in the state of equilibrium is shown in part (a), time-averaged fringes of angular oscillations with a=0.024 and a=0.028 are shown in parts (a) and (d) respectively, a contrast enhanced images are shown in parts (b) and (e).

4. Experimental setup and results

A schematic diagram of the experimental setup is given in Fig. 6. The experimental setup comprises low frequency generator (1), electromagnetic oscillator (2), a disk attached to the planar crankshaft mechanism (3), and a DSLR camera (4). The amplitude and frequency of the generated signal can be manually adjusted by handles (1a) and (1b) of the low frequency generator. The output signal is a harmonic function. The frequency generator is connected by a cable to the electromagnetic oscillator which is attached to a solid metal base (2a). The planar crankshaft mechanism (3) is attached to the same foundation. The electromagnetic oscillator drives

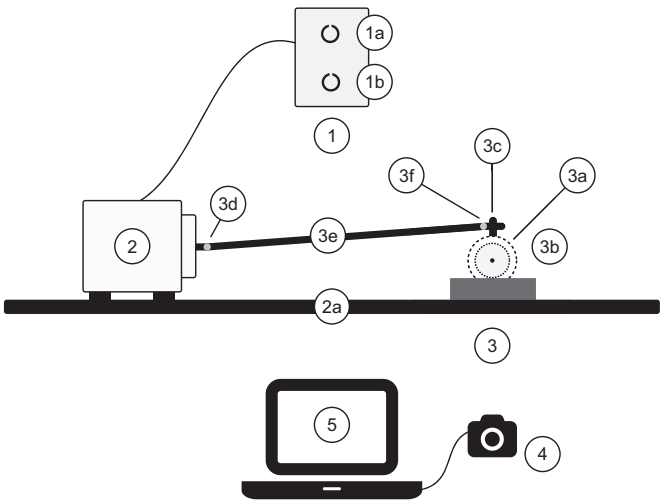

Fig. 6. Scheme of experimental setup: low frequency generator (1), amplitude handle (1a), frequency handle (1b), electromagnetic oscillator (2), solid metal foundation (2a), disk attached to planar crankshaft mechanism (3), planar crankshaft (3a), disk (3b), fixation hinge (3c), fixation joint (3d), metal rod (3e), fixation join (3 f), DSLR camera (4), and computer (5).

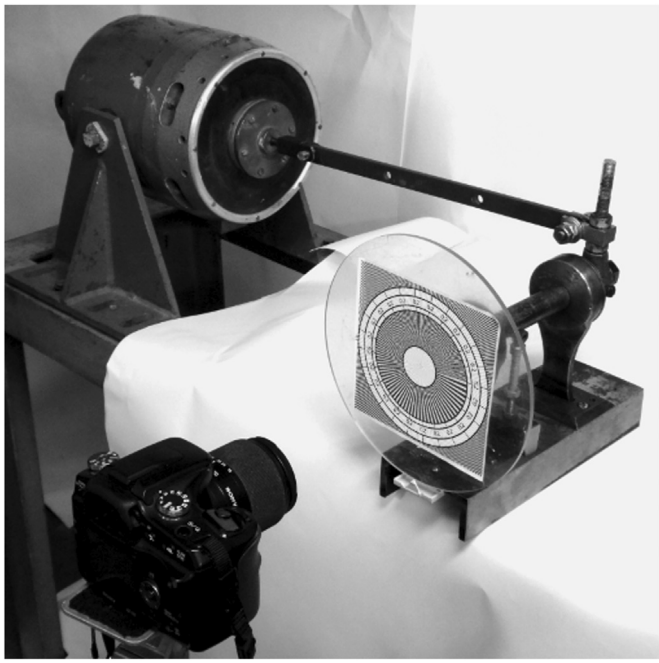

Fig. 7. Experimental setup which comprises: comprises low frequency generator (1), electromagnetic oscillator (2), disk attached to planar crankshaft mechanism (3), and DSLR camera (4).

the planar crankshaft mechanism using the metal rod (3e) with joints (3d) and (3f) that are attached at both ends of the rod. The planar crankshaft mechanism is connected to the electromagnetic oscillator in such a way, that longitudinal core axis of electromagnetic oscillator would align to the axis of metal rod (3e) which is perpendicular to the longitudinal axis of planar crankshaft (3a). This connection method ensures the rotation symmetry of the disk (3b), which is attached to the planar crankshaft (3a). Moreover, this connection method transforms longitudinal oscillations produced by electromagnetic oscillator to angular oscillations of the disk, where the rotation angle can be adjusted by mechanically changing the vertical position of joint (3f) (Fig. 7).

The cover image comprising the circular moiré grating is printed on a glossy white self adhesive sticker paper. There are no specific requirements for the number of image pixels as long as the grating is clear and sharp. In general the main requirement is that the constituting lines of the stationary moiré grating should be not granulated due to poor resolution of the cover image. The rotation axis center of the circular grating is aligned to the rotation axis of disk (3b) (note that incorrect alignment of rotation axis can result in poor time-averaged image). The DSLR camera is attached to a tripod and placed in front of the oscillator disk at a distance of 0.3 m. The optical axis of DSLR camera is aligned to the center of the circular grating. One of the features of the proposed technique is that time-averaged moiré fringes do form directly in the plane of the oscillating cover image. In other words, the formation of time-averaged fringes does not depend on the angle of observation. Analogously, the distance of the camera from the oscillating cover image should ensure that the size of the observed angular scale is sufficient for the identification of the centerline of the time-averaged fringe. Focus, frame size and exposition time (1 s) are adjusted to produce a time-averaged image [13]. The lighting of the crankshaft mechanism should be taken in consideration in order to minimize shadows and reflections. The frequency of the generator is set to 20 Hz. The amplitude of the signal, applied to the electromagnetic oscillator, is chosen in such a way that the amplitude of angular oscillations of the disk is equal to a=0.0235. Time-averaged experimental image is shown in Fig. 8. It can be seen that the centerline of time-averaged moiré fringe corresponds to a preselected amplitude value in the angular scale. Really the pitch of the circular grating at this angle ($\varphi = 63°$) is $\lambda = 0.0267$; thus the time-averaged moié fringe corresponds to the first root of the zero order Bessel function of the first kind according to Eq. (7). As seen in Fig. 8(b), an experimental image can be distorted by various irregularities and noise. Nevertheless, the identification of the centerline of the time-averaged fringe could be performed not only by a naked eye. Semi or fully automatic computational algorithms for the identification of centerlines could assist the operator. A general rule of thumb is that a centerline is located in the area where the fringe extends from inner circle to outer circle.

The proposed experimental technique can be efficiently used for non-destructive optical prediction of degradation of mechanical components performing angular oscillations. For example, angular oscillations of a shaft will start changing if the support bearing starts wearing out. Similary, the amplitude of angular oscillations of a coupling will change if the elastic elements in the coupling gets damaged. Detailed experimental investigations of such degrading structures remains the objective of the future research – but the proposed optical technique offers an efficient approach for such applications.

5. Concluding remarks

A circular moiré grating for measuring amplitude of circular oscillations was constructed in this paper. This scheme considers

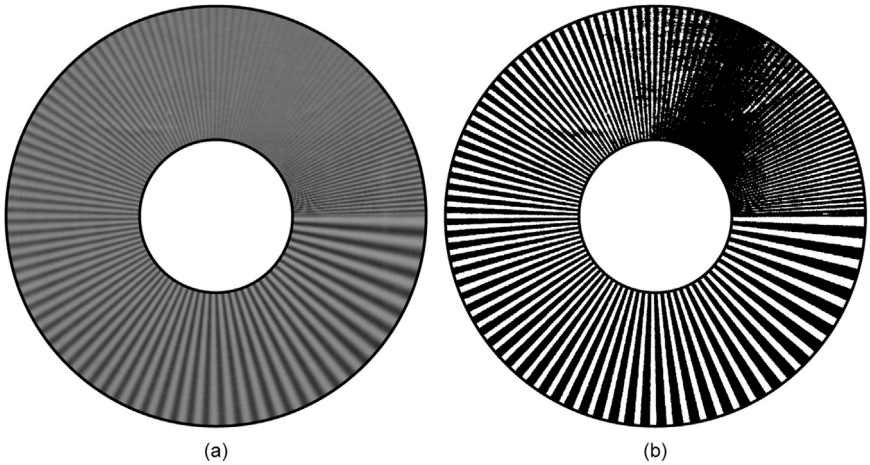

Fig. 8. Time-averaged experimental image corresponding to the angular amplitude a=0.0235. Pitch of the circular grating at angle this angle (φ = 63°) is λ = 0.0267.

angular harmonic oscillations instead of longitudinal harmonic oscillations which are used in standard time-averaged moiré scheme. The cover image (the circular moiré grating) is comprised of concentric circles of dark and white bands around a fixed central point. The circular geometric moiré grating is constructed in such a way, that the angular pitch of the grating depends on the angular coordinate – thus different amplitudes of angular oscillations result into different locations of time-averaged moiré fringes. Such optical effect generated in the time-averaged mode offers a convenient approach for measuring amplitudes of angular oscillations and could be used for degradation prediction of mechanical components performing angular oscillations. Computational simulations as well as experimental results confirm the efficiency and the applicability of the proposed scheme.

Acknowledgements

Financial support from the Lithuanian Science Council under project no. MIP078/15 is acknowledged.

References

[1] A. Kobayashi, S. for experimental mechanics (U.S.), Handbook on Experimental Mechanics, VCH, 1993.
[2] K. Patorski, Handbook of the Moiré Fringe Technique, Elsevier, 1993.
[3] G. Lebanon, A.M. Bruckstein, Energy minimization methods in computer vision and pattern recognition, in: Proceedings of the Third International Workshop, EMMCVPR 2001 Sophia Antipolis, France, September 3–5, 2001, Proceedings, Springer Berlin Heidelberg, Berlin, Heidelberg, 2001, Ch. Designing Moiré Patterns, pp. 185–200.
[4] M. Naor, A. Shamir, Visual cryptography, in: Lecture Notes in Computer Science, Vol. 950, Springer-Verlag, 1995, pp. 1–12.
[5] X. Yan, S. Wang, X. Niu, C.-N. Yang, Halftone visual cryptography with minimum auxiliary black pixels and uniform image quality, Digit. Signal Process. 38 (2015) 53–65.
[6] X. Yan, S. Wang, X. Niu, C.-N. Yang, Generalized random grids-based threshold visual cryptography with meaningful shares, Signal Process. 109 (2015) 317–333.
[7] D. Ou, W. Sun, X. Wu, Non-expansible XOR-based visual cryptography scheme with meaningful shares, Signal Process. 108 (2015) 604–621.
[8] P.-L. Chiu, K.-H. Lee, User-friendly threshold visual cryptography with complementary cover image, Signal Process. 108 (2015) 476–488.
[9] Y.-C. Hou, Visual cryptography for color image, Pattern Recognit. 36 (7) (2003) 1619–1629.
[10] C.-N. Yang, T.-S. Chen, Colored visual cryptography scheme based on additive color mixintg, Pattern Recognit. 41 (10) (2008) 3114–3129.
[11] H. Luo, H. Chen, Y. Shang, Z. Zhao, Y. Zhang, Color transfer in visual cryptography, Measurement 51 (2014) 81–90.
[12] C. Liang, Y. Hung, A. Durelli, J. Hovanesian, Time-averaged moiré method for in-plane vibrational analysis, J. Sound Vib. 62 (2) (1979) 267–275.
[13] M. Ragulskis, A. Aleksa, Image hiding based on time-averaging moiré, Opt. Commun. 282 (14) (2009) 2752–2759.
[14] K. Philipp, A. Filippatos, R. Kuschmierz, A. Langkamp, M. Gude, A. Fischer, J. Czarske, Multi-sensor system for in situ shape monitoring and damage identification of high-speed composite rotors, Mech. Syst. Signal Process. 76 (2016) 187–200.
[15] L. Chen, T. Laifa, F. Huanzhen, W. Zhaobing, Approach to health monitoring and assessment of rolling bearing, J. Vibroeng. 15 (2) (2013) 746.
[16] V.T. Tran, H.T. Pham, B.-S. Yang, T.T. Nguyen, Machine performance degradation assessment and remaining useful life prediction using proportional hazard model and support vector machine, Mech. Syst. Signal Process. 32 (2012) 320–330.
[17] Z. wang Gan, J. Ma, C. Lu, H. Liu, T. min Shan, Real-time reliability assessment and lifetime prediction for bearings using the individual state deviation based on the manifold distance, Trans. Can. Soc. Mech. Eng. 39 (2015) 691–703.
[18] Z. Wang, C. Lu, Z. Wang, J. Ma, Health assessment of rotary machinery based on integrated feature selection and gaussian mixed model, J. Vibroeng. 16 (4) (2014) 1753–1762.
[19] M. Ragulskis, A. Aleksa, J. Ragulskiene, Image hiding based on circular moiré fringes, Wseas Trans. Math. 9 (1) (2010) 90–99.
[20] M. Ragulskis, M.A.F. Sanjuan, L. Saunoriene, Applicability of time-average moiré techniques for chaotic oscillations, Phys. Rev. E 76 (2007) 036208.